Brazilian Journal of Geophysics, 42 (2024), 1. 1-20
Brazilian Geophysical Society
ISSN 2764-8044
DOI: 10.22564/brjg.v41i1.2295

3D REFRACTION TRAVEL TIME ACCURACY STUDY IN HIGH CONTRASTED MEDIA

Paulo H. B. Alves [1*], Luiz A. Santos [1,2],
Felipe V. Capuzzo [1], and Marco Cetale [1]

[1]Universidade Federal Fluminense – UFF, Programa de Pós-Graduação em Dinâmica dos Oceanos e da Terra – PPGDOT, Grupo de Imageamento Sísmico e Inversão Sísmica – GISIS
[2]Petrobras

*Corresponding author email: pbastos@id.uff.br

ABSTRACT

Among all the existing methods to solve the eikonal equation, three methods are chosen to verify accuracy, symmetry, reciprocity and error propagation along large offsets of refracted waves in seismic near surface exploration context. Performance is extremely highlighted nowadays and accuracy is being neglected, then an eikonal solver poorly explored in geoscience is used. A classical solver, the Fast Iterative and the modified Fast Sweeping Method are applied in three modeling schemes: a simple two layers model, a large four layers and a complex benchmark model. The three methods compute the first arrival of refracted waves in high contrast media and the results are compared to the analytical solution. A circular geometry is considered in all experiments to explore the method applicability using full azimuth angles. On the first scheme, the errors in travel time are computed among the three methods using different model sample spacing and we discuss accuracy, symmetry and reciprocity of first arrivals. On the second scheme, three circular receivers are placed in different offsets to check errors along refracted wave propagation. Finally, the third scheme, four shots are strategically positioned over the SEG/EAGE Overthrust model in order to compare the full acoustic wavefield with the eikonal solvers and then check the similarities. Although the focus is on methods accuracy, the algorithm run time is also considered and the comparison shows that the modified Fast Sweeping Method is the most accurate. The most computational efficient eikonal solver is the Fast Iterative Method, but its geoscience applicability needs to be cautious, because of its inaccurate results.

Keywords: eikonal solvers; refracted waves; numerical - analytical comparison; accurate first arrivals.

INTRODUCTION

There is a number of refracted wave applications in exploration seismology such as migration (Shen and Zhang, 2020), illumination study to reservoir monitoring (Lopez et al., 2020) and, most often, in seismic tomography. Comparing eikonal and ray tracing based tomography in cross well survey Balkaya et al. (2010) conclude that the eikonal kernel inversion obtains better reconstruction of sharp structures. Besides, Farra (1993) shows that a smoothed model is the solution for instability of ray tracing equations, and due to this, eikonal equation is highly recommended to compute travel times in strongly contrasted media. An iterative solution for eikonal equation is developed by Vidale (1988) and then, novel solvers are proposed (Van Trier and Symes, 1991; Podvin and Lecomte, 1991; Qin et al., 1992; Hole and Zelt, 1995). Currently efforts are being directed to the wavefront expansion solvers such as Group Marching Method (Qin et al., 1992), Fast Marching Method Sethian (1999) and Fast Iterative Method Jeong and Whitaker (2008). The Fast Sweeping method appears as a great solver as it is

demonstrated in Capozzoli et al. (2013), whose study compares time execution of Fast Marching, Fast Iterative and Fast sweeping methods in homogeneous media and in a maze model. The Fast Iterative Method performs better than the others, but nothing is shown about accuracy. The strategy of using refracted waves with large offset shot circles in Ocean Bottom Nodes geometry are being applied to monitoring and characterize reservoir in pre-salt Brazilian Santos basin (Lopez et al., 2020; Costa et al., 2020; Da Silva et al., 2022). Following this acquisition geometry, but using refracted travel times, the objective of this paper is to verify eikonal solvers accuracy and reciprocity of three methods: the classic (Podvin and Lecomte, 1991), the fast iterative method (Jeong and Whitaker, 2008) and a variation of fast sweeping method (Noble et al., 2014) comparing with an analytical solution for refracted waves. Reciprocity is taken into account because in Tryggvason and Bergman (2006) have shown a discrepancy error in classical methodology and then a solution is proposed. The application of an accurate method in high contrasted media could bring more information in inversion and migration.

Firstly, in the following section, we describe equations, methodology and detail the modeling schemes to compare analytical and numerical solution of travel times. The first approach is the most simple to verify symmetry, reciprocity and precision of first arrival travel times. The second approach is used to verify travel time errors along offsets, so interfaces are strategically positioned to pick the time at each circle geometry. Third, and last scheme, illustrates the wave propagation comparison with first arrivals in SEG/EAGE Overthrust model. Thus, the acoustic wave equation is solved using finite difference stencils and the first arrival amplitude is compared with first arrival travel times. The Results and Discussion sections show all figures to verify the simulations and although the focus of this work is the accuracy of the methods, we discuss the computational time in each experiment. Finally, the Conclusion section points out the considerations of the analysis in accuracy and performance for each experiment and methods.

MATERIALS AND METHODS

The target phenomena to be studied in this research are the head waves, the one that are refracted whenever the incident angle is higher than the critical angle (Sheriff and Geldart, 1995). We can generate head waves using the high frequency approximation of wave equation for isotropic and acoustic media, the Eikonal equation

$$\left(\frac{\partial T}{\partial x}\right)^2 + \left(\frac{\partial T}{\partial y}\right)^2 + \left(\frac{\partial T}{\partial y}\right)^2 = \frac{1}{v^2(z,x,y)}, \tag{1}$$

where $T = T(z,x,y)$ in 3D case, is the first arrival volume and $v = v(z,x,y)$ velocity model, $v(z,x,y)$. Because we are considering the isotropic formulation, the ray is orthogonal to the wavefronts and may be calculated as the gradient of travel time volume (Robinson and Clark, 2017). The first arrivals correspond to the exact solution of an elastodynamic equation and build a complete wavefield based on known velocity model (Cervenỳ, 2001). Therefore, the eikonal solvers try to apply numerical methods to solve the spatial partial derivatives over travel times present in equation 1. The most famous methodology is the Finite Difference Method that approximate the derivatives using the Taylor series function over model grid points depending on the approximation order. Different of classical wave equation solution, the operators are built considering the near neighbours grid points and to improve accuracy authors use more neighboring points (Ahmed et al., 2011; Cai et al., 2023).

Analytical solution

A general formulation is used to calculate analytical travel times for n horizontal layers (Kearey et al., 2002). Distance between source and receiver (offset), 1D velocity model and thickness of all layers are needed. The main equation is given below

$$t_n = \frac{x}{v_n} + \sum_{i=1}^{n-1} \frac{2z_i \cos(\theta_{in})}{v_i}; \quad \theta_{in} = \sin(v_i/v_n), \tag{2}$$

where t_n is the travel time for each layer n, x is the offset, z_i and v_i are the thickness and the velocity of each layer i respectively and θ_{in} is the incident critical angle for each layer. Generalization scheme and a simplification for three layers is shown on Figure 1. This scheme is used to compute analytical travel times to compare with numerical solutions described in next sections.

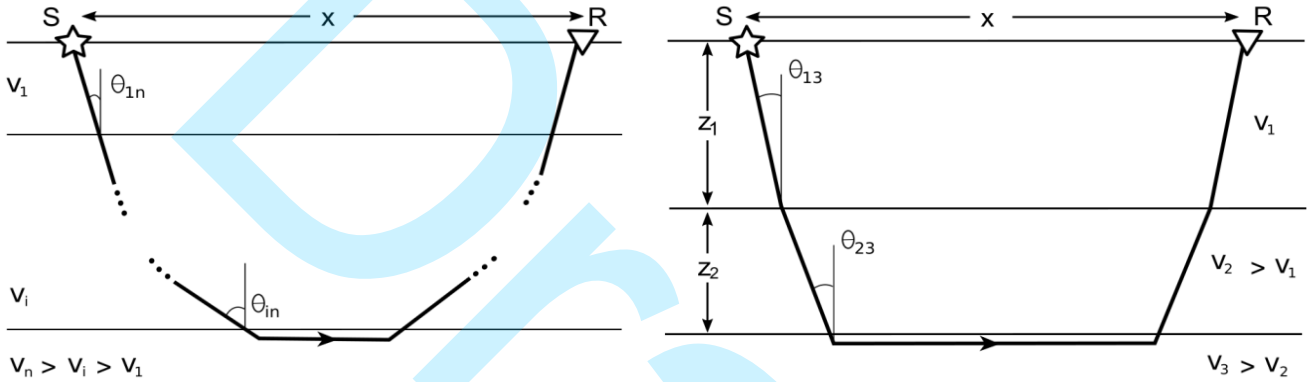

Figure 1: a) Analytical solution for n planar layers. b) Simplification for three layers adapted from Kearey et al. (2002). S to reference the source position and R to show receiver position, both on the same elevation. x is the offset and z the thickness of each layer. θ is the incidence critical angle related with interface velocity contrast. Velocity always increase with depth and there is no lateral velocity variation inside each layer.

Classical method

The method chosen to be the main reference for this study is Podvin and Lecomte (1991) formulation. This methodology is broadly used to compute first arrival travel times in geoscience problems. Linde et al. (2008) performs a 2D joint inversion using structural constraints, Yordkayhun et al. (2009) maps through 3D travel time tomography to monitoring CO_2 migration in a saline aquifer, De Matteis et al. (2010) explores a statistical analysis to estimate model uncertainty and resolution in 3D first arrival tomography and Bulhões et al. (2021) study the regularization effects using first arrival tomography in shallow models. All those works are related to inversion problems, but using Podvin and Lecomte (1991) formulation as the modeling kernel. Despite the high applicability, some limitations can be found, such as in Tryggvason and Bergman (2006), where discrepancies in the calculation of times using reciprocity, and Koketsu (2000), where instability of times using models with irregular interfaces could be found.

Based on the finite difference approximation, the classical method uses a systematic application of Huygens principle, where each wavefront expansion can behave as a source that expand another wavefront. Because of that, causality is respected in propagation. This numerical method discretizes equation 1 and build finite

difference operators that can use the neighboring points to derive 1D, 2D and 3D operators. The model is constructed as a regular grid volume, and some of conditional operators are applied to check illumination at each grid point computed. In the 3D case computation, up to 170 stencils are applicable: six 1D transmitted arrivals, twenty four 2D transmitted arrivals (conditional), twelve 2D diffracted arrivals, ninety six 3D transmitted plane wavefront (conditional) and thirty two 3D diffracted arrivals (Podvin and Lecomte, 1991). The number of iterations is computed based on the distance from the source position to the end of the model in samples. An auxiliary volume is stored at each iteration to save grid points that have been computed using the expanding cube methodology. All finite difference operators are computed in order to find the smaller travel time. It is necessary to compute the analytical travel time from source to the nearest grid point in meters to compute the first arrivals outside a grid point. Trilinear interpolation is applied to register time at the receiver outside the grid point. The process to compute travel times at each grid point is independent, so parallel computing is possible. Thus the algorithm is parallelized using OpenACC compilation directives on C++ programming language (Farber, 2016).

Fast iterative method

The Fast Iterative Method (Jeong and Whitaker, 2008) improved the performance of eikonal equation solvers, and it was inspired by the Fast Marching method (Sethian, 1999) and others wavefront expansion methods. This methodology is highly used in GPU parallelization approach, and many benchmark execution time tests are available in different parallel distributions. Dang and Emad (2014) investigate two parallel level approaches working with asynchronous communication. Hong and Jeong (2016) solve the method using multi-GPU system, and Huang (2021) manages the algorithm to improve performance of the method. All those works prioritize only performance. The Fast Iterative Method tries to formulate a cheapest alternative algorithm that beats the famous and broadly applied geoscience Fast Marching Method because of its simplicity and high performance. The Sethian (1999) method is broadly developed such as Rawlinson and Sambridge (2004, 2005) and show the availability to handle wave propagation in heterogeneous media. Herrmann (2003); Yang and Stern (2017) use domain decomposition to make Fast Marching method parallelizable. Although Cai et al. (2023) has tested the accuracy and proposed an improved formulation, the methodology of Jeong and Whitaker (2008) have not been compared with other formulations in terms of accuracy.

The Fast Iterative Method was chosen because Capozzoli et al. (2013) show its higher computational performance over the Fast Marching Method for a homogeneous medium. Despite we record run time experiments, we focus our study on the accuracy of the calculated travel time. The Fast Iterative Method kernel equation is empirically formulated based on well-known eikonal equation solvers (Jeong and Whitaker, 2008). The algorithm proposes a list scheme: the updated points, the wavefront points (active list) and the external points. The iterative process solves the equation only using the wavefront points, avoiding computational effort in all grid points. The active list, at the beginning of simulation, contemplates only the nearest source neighboring points. After the update, the active list is emptied, new points are added to the active list, and a new iteration starts in a process such as wavefront expansion. In this study, the original scheme of lists is not employed. To propagate travel times using the Fast Iterative Method, only the kernel equation and the expanding cube methodology are applied. In our implementation, to initialize a source outside grid points we compute analytical time from the

source position to the nearest grid point in meters, and we register travel time outside grid points, performing a trilinear interpolation.

Accurate Fast Sweeping Method

The Fast Sweeping Method, originally created by Zhao (2005), is an iterative formulation to improve finite difference operators to compute eikonal solvers. The method sweeps the entire 3D domain in different directions reducing computational cost on serial computing when compared to Podvin and Lecomte (1991) formulation that solve the operators in cascade. Bak et al. (2010) show how Fast Sweeping Method can be better than Fast Marching Method in strong velocity contrasts using some sweeping domain variations. Zhao (2007) illustrates the first attempt of parallelized Fast Sweeping method and Detrixhe et al. (2013) show that the Zhao (2007) method cannot be parallelized on large scale, and proposed a better solution that solves the problem efficiently. The Fast Sweeping Method is broadly applied using anisotropic media (Luo and Qian, 2012; Waheed et al., 2015; Waheed and Alkhalifah, 2017; Huang and Luo, 2020) with great feasibility for realistic applications. Focusing on accuracy, Noble et al. (2014) create an hybrid Accurate Fast Sweeping Method for eikonal equation on isotropic media using Spherical and Cartesian finite difference operators. The main innovation of this method is the expanded 8 point finite difference operator originally from Vidale (1988), that shows in truncated form. The spherical operators are applied near from source to fit the wavefront spherical behavior and the cartesian operators are applied over other grid points far from source. With the expansion of 8 points Vidale (1988) operator, the precision increase and some operators could be discarded to improve execution time (Noble et al., 2014). In this paper, just the Cartesian operators is used with no parallelization following the 3D code on Noble et al. (2014) github's repository. An important aspect to emphasize about Noble et al. (2014) formulation is that the points around the source need to be initialized with analytical travel times. There is a step before the global sweep that sweeps domain using source position as the reference to start sweeping until the edges of domain called initial sweep. This step makes the Fast Sweeping Method converge in only one iteration for most of the average subsurface models. As in other previous methods presented in this paper, the receivers outside the grid is registering travel times using a trilinear interpolation of neighboring points.

Modeling schemes

The first scheme of this study is related with symmetry and reciprocity accuracy analysis. Thus, a simple model is applied and the sample spacing is changed to verify the effects of the grid size. The common used discretization parameters applied are 100, 50 and 25 meters [m]. The model dimension, considering (z, x, y) format, are (1.1, 22, 22) kilometers [km]. The total samples of models are (12, 221, 221), (23, 441, 441) and (45, 881, 881) homogeneous grid for spacing of 100, 50, 25 m respectively. Figure 2, shows the acquisition geometry, a velocity log and vertical model slices to illustrate all approach 1 configuration. The acquisition geometry has 5 shots positioning at 1 - (0, 1, 1), 2 - (0, 1, 21), 3 - (0, 21, 1), 4 - (0, 21, 21) and 5 - (0, 11, 11) km. Shots are strategically positioned to verify symmetry between shots 1 with 3 and 2 with 4. Shot 5 is used to verify reciprocity propagation, when receiver and shot position are inter-changed. The receiver configuration is circular, the center is located at (0, 11, 11) km with 10 km of radius and 12.5 m of circular distance between them.

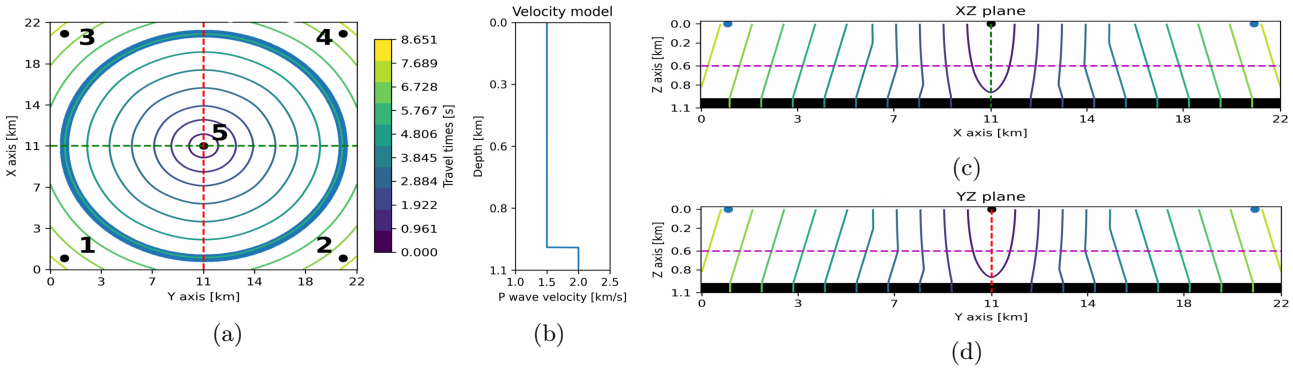

Figure 2: First scheme. a) acquisition geometry with shots and receivers position, travel times are the contours and dotted lines indicate plane slices. b) 1D velocity model illustrating depth interface. c) and d) travel times contour and the projection of central shot and receivers at XZ and YZ plane slices are shown.

The second scheme analyze errors during wavefront propagation between layers. Figure 3, shows the entire configuration of how acquisition geometry was chosen, velocity model interfaces and ray path distribution at each layer. The model dimensions are (4.5, 27, 27) km, in (z, x, y) format, the sample spacing is 25 m and the model has (181, 1081, 1081) samples. Just one source at center of the model is applied to check all azimutal signature of travel times. The layer interfaces is located at 1, 2.4 and 4.2 km from up to bottom, and the velocities are 1.5, 2, 3 and 4.5 km/s. Three circular geometry are applied with 12.5 m equidistant receivers. All circles are centered at position (0, 13.5, 13.5) km and they have 880, 1257 and 1634 receivers for 7, 10 and 13 km of circle radius respectively. The analytical formulation gives the travel times per layer, so in order to compare analytical and numerical travel times, it is necessary to register only the smaller times using all interfaces as shown in Figure 3 d), where the purple line is the target of analytical times. Ray path are shown in Figure 3 c) and they are calculated from the gradient of the transit time volume, for isotropic media, is perpendicular to the isochrones (Vidale, 1988). We apply the descent gradient method to find ray path from receiver to source with fixed ray step of 25 % of minimal grid length.

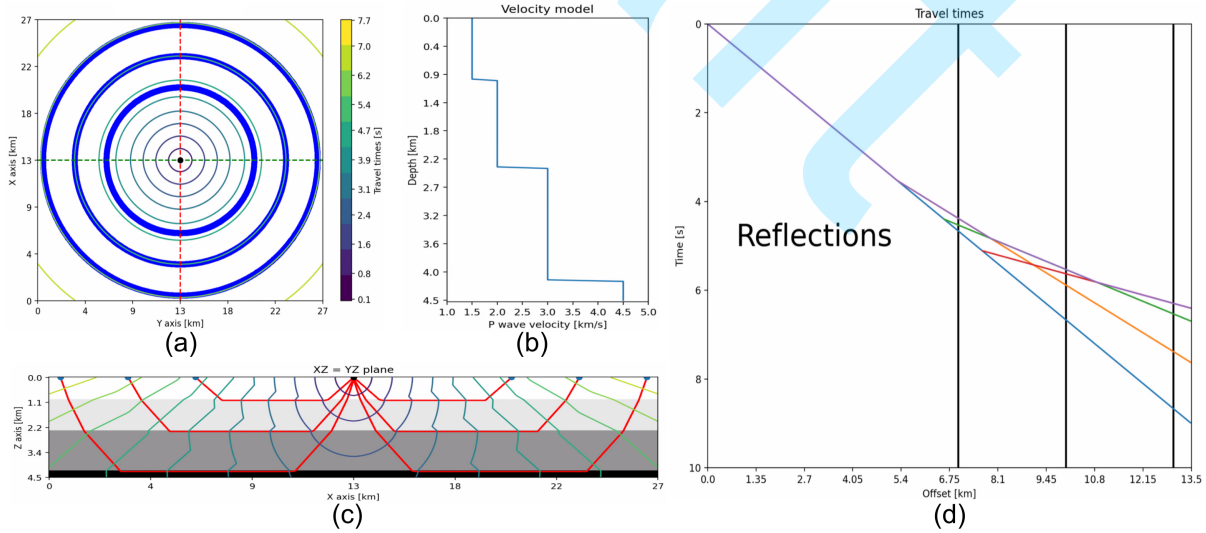

Figure 3: Second scheme. a) all acquisition geometry with receiver circle radius of 7, 10 and 13 km. Travel times are delimited by a contour map. b) 1D velocity model to show velocity contrasts at each depth. c) 2D model slice to show ray paths from source to projected receivers. d) Circle offset justification, for each circle a different wavefront is registered, the smaller time is selected to build first arrival travel times.

In the third scheme, we study how numerical first arrivals can be correlated to waveform modeling for acoustic media performing on the SEG/EAGE Overthrust model (Lecomte et al., 1994). A smoothed version of this model is used in Noble et al. (2014) to verify accuracy of a new eikonal solver. In our study we use a version of the model without smoothing to verify wavefront similarities between acoustic wave equation and numerical first arrivals. The model dimension is (4.66, 20, 20) km and the sample spacing is 12.5 m to use frequencies high enough to perform numerical simulation with a manageable model, which is (373, 1601, 1601) samples and almost 4 GB of storage. Figure 4 shows the third scheme configuration of the circular acquisition geometry, a central log velocity and the vertical slices of XZ and YZ plane. The velocities on the model varies from 2.5 to 6 km/s. The acquisition geometry is composed with 4 shots and 1194 receivers. Shots are positioned at 1 - (0, 0.5, 0.5), 2 - (0, 19.5, 0.5), 3 - (0, 0.5, 19.5) and 4 - (0, 19.5, 19.5) km and receivers are on circular configuration spaced 50 m each other. Circle is centered at (0, 10, 10) km and the radius is 9.5 km. The nearest offset is 3935 m and the larger offset is 22935 m for all shots position.

Wave equation for isotropic acoustic media is given by

$$\nabla^2 P - \frac{1}{v^2}\frac{\partial^2 P}{\partial t^2} = f(t), \tag{3}$$

where $P = P(z, x, y)$ is the pressure in Pascal [Pa], $v = v(z, x, y)$ is the velocity model volume and $f(t)$ is a source applied at (z_0, x_0, y_0) position on time instant t. The reference source is a zero phase Ricker wavelet with 50 Hz of maximum frequency and 1 Pa of maximum amplitude. The finite difference method is applied and we employ operators with eighth order in space and second order in time. Boundary conditions was solved using a classical absorbing condition (Cerjan et al., 1985) with 50 points and attenuation coefficient of 0.0045 following Bording (2004) that shows the optimal way to set parameters in sponge boundary condition. We record waveform outside the grid using the Hicks (2002) interpolation. Total modeling time is 6 seconds and discretization parameter is 0.8 ms to avoid finite difference numerical dispersion and maintain stability conditions.

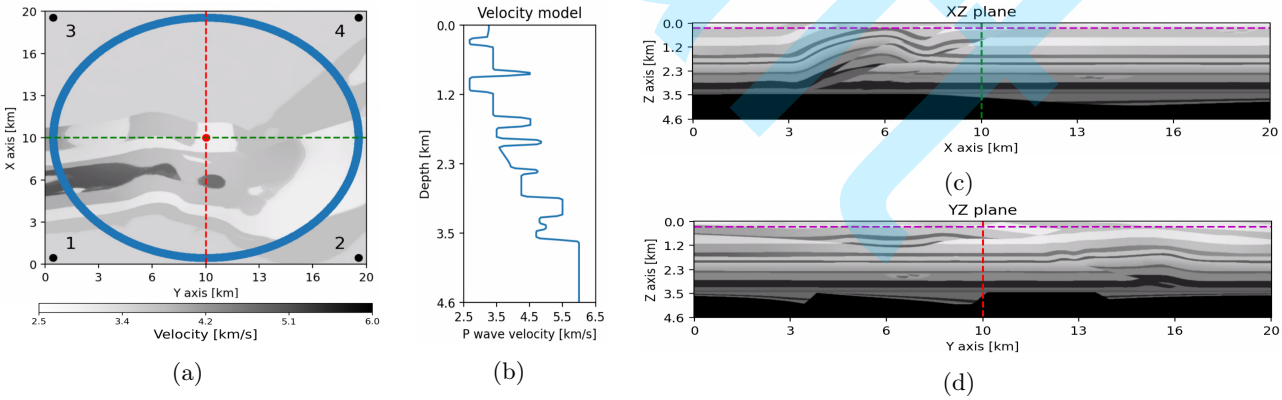

Figure 4: Third scheme: SEG/EAGE Overthrust benchmark model. a) acquisition geometry with shots and receivers position. The color bar represents all velocities in the model. b) 1D velocity model log projected at the center of the model. c) and d) is the model XZ and YZ projection, dotted lines indicate each projection.

All the results will respect the same color scheme for each eikonal solver, which is blue for Podvin and Lecomte (1991), yellow for Jeong and Whitaker (2008) and green for Noble et al. (2014). The line styles for each model discretization parameter are solid, dashed and dash-dotted for 25 m, 50 m and 100 m respectively.

RESULTS AND DISCUSSIONS

Each scheme is discussed individually to explain their particularities. Scheme 1 shows the results about symmetry and reciprocity analysis in order to measure azimutal errors and numerical time errors. Scheme 2 illustrates how travel time errors behave when wavefront propagates in high contrasted velocity interfaces. Scheme 3 presents the acoustic waveform propagation comparing to numerical eikonal solutions in order to verify correlations between them.

First scheme

All the base results of the first scheme are illustrated in Figure 5, where the shot gathers for each shot position are shown in a global view (Figures 5 a), b), c) and d)) for symmetry studies and in a refined view (Figures 5 e) and f)) for accuracy and reciprocity studies.

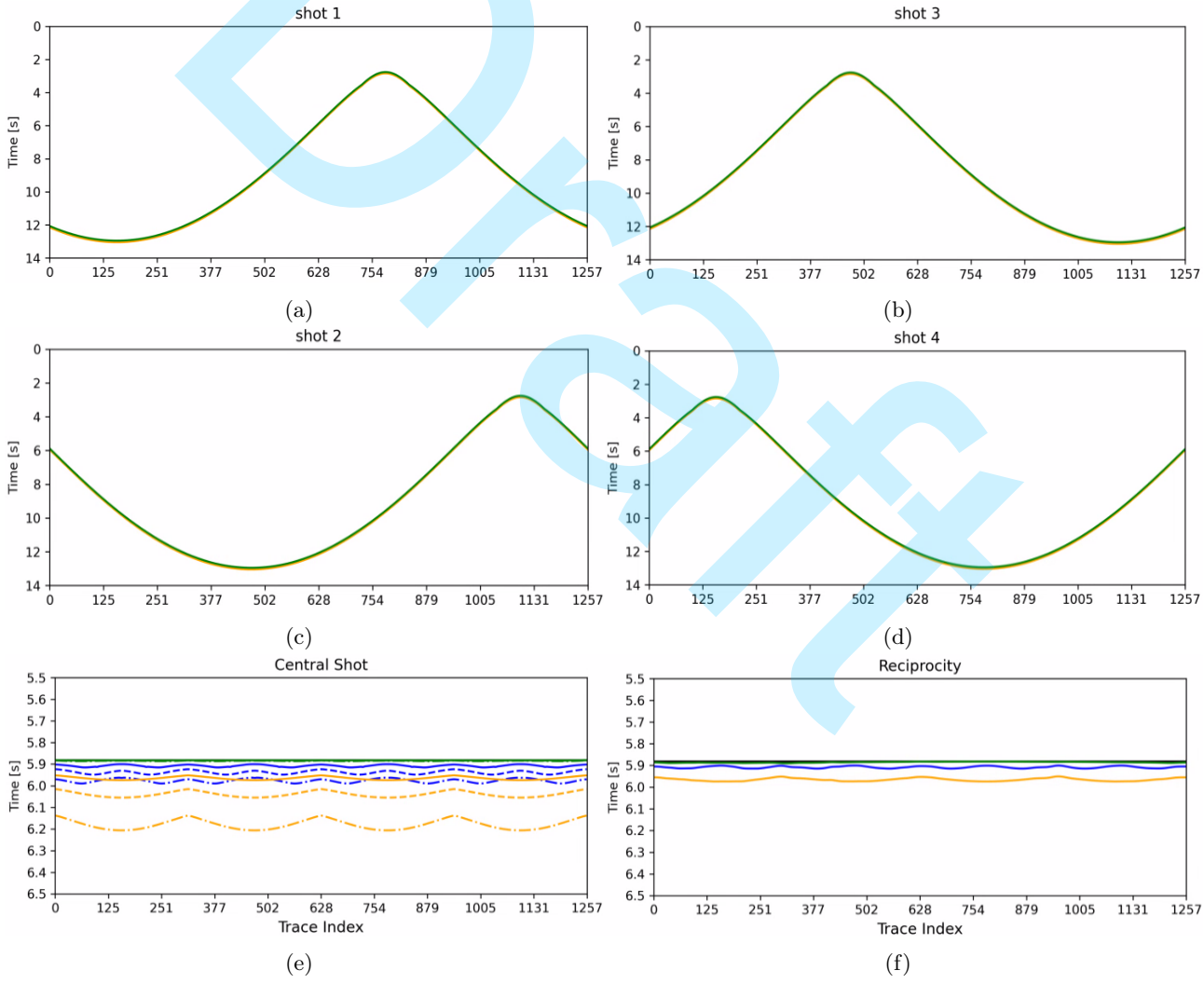

Figure 5: First scheme. Shot gathers for position 1 (a), 3 (b), 2 (c) and 4 (d) to build the symmetry studies. Shot gathers for the central position (e) and (f) to build the reciprocity and detailed accuracy studies. The colors indicates the methods and the line style indicates the model sample spacing. About the colors we have blue for Podvin and Lecomte (1991), yellow for Jeong and Whitaker (2008) and green for Noble et al. (2014). About the line styles we have solid for 25 m, dashed for 50 m and dash-dotted for 100 m. The reciprocity study only was done using the model with spatial discretization parameter of 25 m.

The symmetry analysis about symmetric shots following the acquisition geometry in Figure 2 is presented in Figure 6. The vertical axis is the time error in milliseconds and the horizontal axis is the receiver indexes of a circular configuration. The symmetry study was done using the results of Figure 5 a) subtracted by the travel times in Figure 5 b) in its reverted indexation. This operation is shown on Figures 6 a), c) and e) for sample spacing of 100, 50 and 25 m respectively. The same analysis was done for the other pair of symmetrical shots illustrated in its raw form in Figures 5 c) and d), which the results are shown in Figures 6 b), d) and f). The eikonal solvers respected the symmetry employed by the acquisition geometry, just the Podvin and Lecomte (1991) formulation 25 m sample spacing case that appeared some noise in a scale of 1 millisecond. It shows that the travel times are being computed equally in entire circular geometry independent of geometry direction. That is a great information to use eikonal equation in target oriented reservoir monitoring studies with circular geometry.

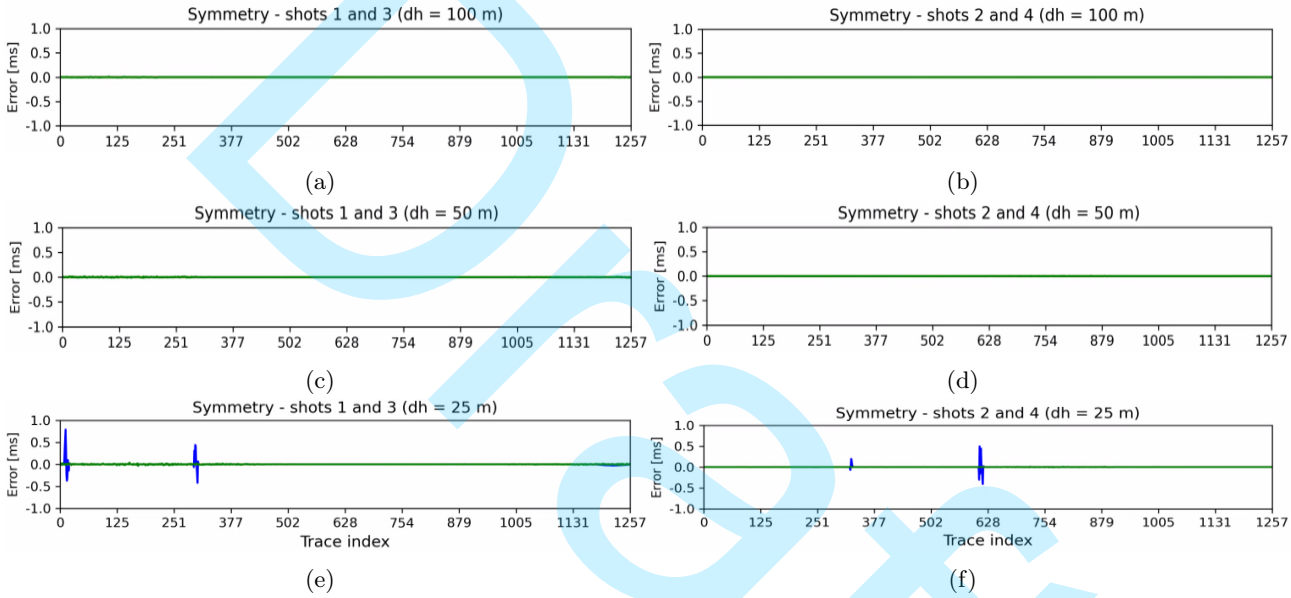

Figure 6: Symmetry results for the first scheme. a), c) and e) are the symmetrical shots analysis for positions 1 and 3 with discretization parameter of 100 m, 50 m and 25 m respectively. b), d) and f) are the symmetrical shots analysis for positions 2 and 4 with discretization parameter of 100 m, 50 m and 25 m respectively. The color convention of eikonal solvers is applied, but the resulted lines are overlapped. e) and f) present some noise artifacts but is smaller than common seismic exploration resolution.

The regional accuracy study is done by computing the analytical solution subtracted by the numerical formulations for each discretization parameter shown in Figures 5 a), b), c) and d). To optimize the figure, the symmetrical shots will be plotted at the same image where for shots 1 and 2 the line style is solid, and for shots 3 and 4 the line style is dashed with opacity. Figure 7 shows the accuracy of travel times for external shots 1,2,3 and 4. This analysis is possible subtracting the analytical solution by the numerical results for each eikonal solver using specific model sample spacing. Figure 7 presents the results with the same scale to show that travel time errors decrease with discretization parameter refinement. It happens just because of finite difference operators can generate better results with thin grid spacing. Note that the formulation with larger difference between analytic errors is the Fast Iterative Method and the formulation with the smaller errors is the accurate Fast Sweeping Method. The four external shots run time for each numerical method are registered in Table 1. According to the Table 1 results, the fastest algorithm is the Fast Iterative method. The classical formulation

appears not so computationally efficient with the 100 m of sample spacing, but when the discretization parameter decreases it becomes faster than the Fast Sweeping Method. It is the implication of the hardware used to compute each method, when GPU is activated, lager parallel processes work better than larger serial processes. The storage model is counting total grid points divided by 1 Mega Byte, for example a 25 m model has $45 \times 881 \times 881 \times 4 \,/\, 1024 \,/\, 1024 \approx 133$ MB.

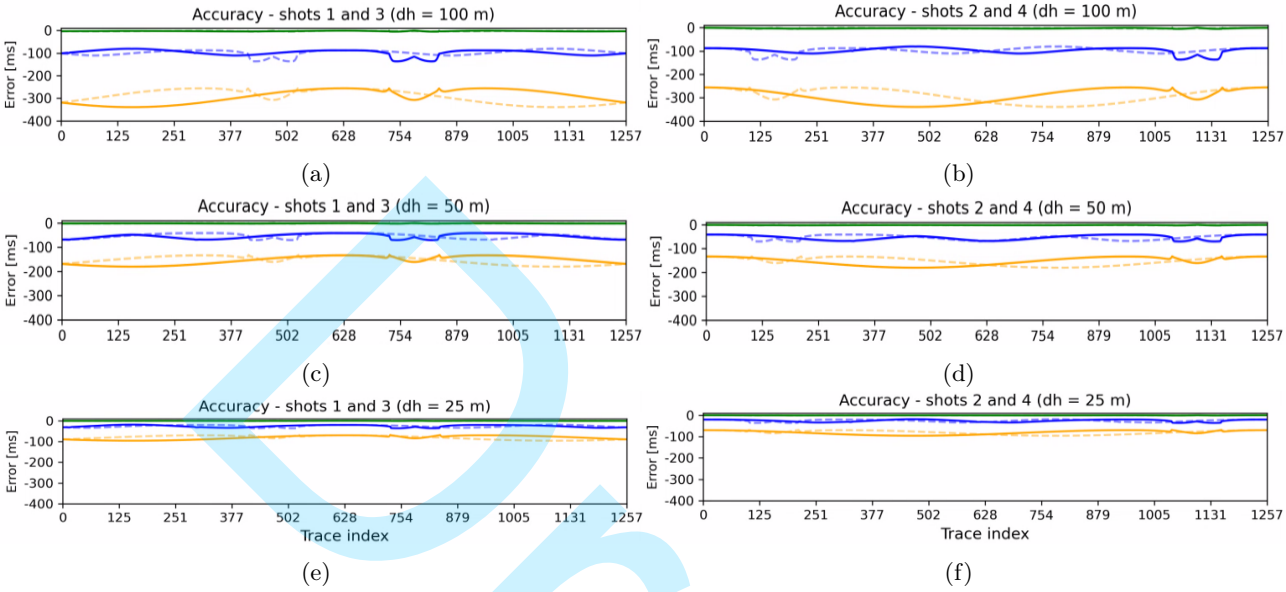

Figure 7: Accuracy results for external shots of the first scheme. a), c) and e) are the shots 1 and 3 accuracy respecting the color and line style convention: Blue for Podvin and Lecomte (1991), yellow for Jeong and Whitaker (2008) and green for Noble et al. (2014). The solid lines represent the shots 1 and 2 errors, on the other hand the dashed lines represent the shots 3 and 4 errors. The scale of errors are the same to validate the error decreasing with grid refinement.

Table 1: Execution time for external shots on first approach and the storage of each model.

	100 m	50 m	25 m
Podvin and Lecomte (1991)	4.469 s	5.557 s	60.269 s
Jeong and Whitaker (2008)	0.523 s	3.761 s	53.408 s
Noble et al. (2014)	2.485 s	12.113 s	92.937 s
Model storage	2.2 MB	17 MB	133 MB

The central shot of the first scheme with the accuracy and the reciprocity study is shown separately where Figure 8 shows only the accuracy results and Figure 9 shows the reciprocity results. The expected behavior of circular geometry survey with a central shot results is a constant travel time as the analytical solution computes. The analytical equation show that for central shot the travel times response is a constant time for all receivers. Looking at Figures 8 a), b) and c) carefully, the maximum difference error registered occurs in -120, -350 and -5 ms respectively. Because of that, the most accurate method is the Noble et al. (2014) formulation for this case due to the magnitude of difference between analytical and numerical solutions.

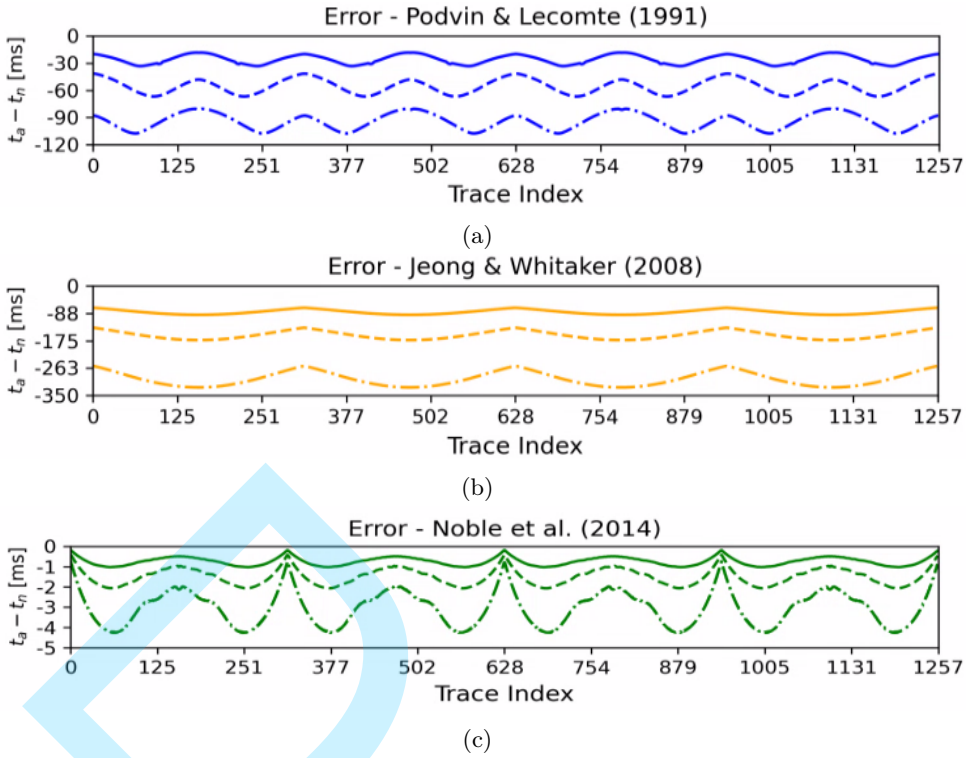

Figure 8: Central shot error comparison for the first scheme. a) Podvin and Lecomte (1991), b) Jeong and Whitaker (2008) and c) Noble et al. (2014) formulations. The line styles represent the model sample spacing, where solid lines are for 25 m, dashed for 50 m and dash-dotted for 100 m spacing.

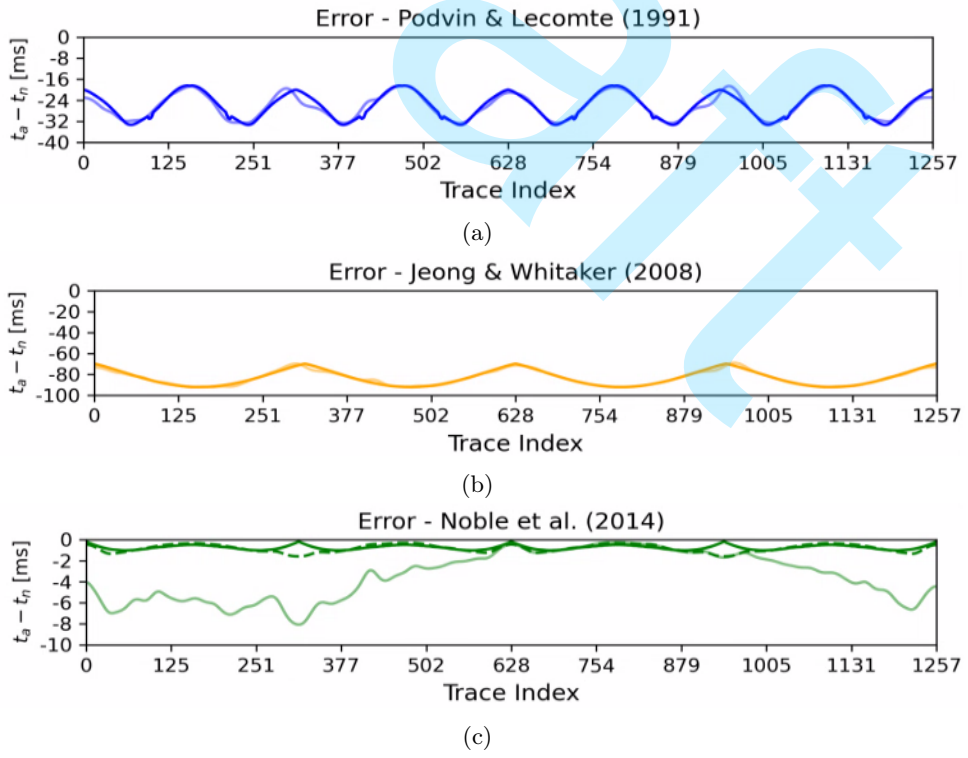

Figure 9: Reciprocal time accuracy study for the first scheme. Solid lines represent the shot to receiver records and opaque lines the receiver to shot records. a) Podvin and Lecomte (1991), b) Jeong and Whitaker (2008) and c) Noble et al. (2014) formulations. The dashed line in part c) represents the adjusted travel times caused by a wrong initialization in Noble et al. (2014) algorithm.

Figure 9 shows the reciprocity travel time errors behavior of 25 m sample spacing comparison. The results in Figures 9 a) and b) fit well between forward and reciprocity travel times and in Figure 9 h) the difference had huge errors initially. These errors are caused because Fast Sweeping Method was not initialized perfectly at all possible directions. When we start the eikonal solution, an initialization is compute the analytical travel time to fill all points surrounding the source with exact solution. After that, the travel times respect the reciprocity principle very well (Figure 9 c) - dashed line). The sinuous behavior in all travel times is because the Cartesian coordinate has an intrinsic azimutal imprecision (Alkhalifah and Fomel, 2001; White et al., 2020). The run time of central shot for all numerical methods and the reciprocity run time for 1257 shots are shown in Table 2. Estimated reciprocity run time is computed based on the run time of 25 m sample spacing.

Table 2: Execution run time for central shot on first approach and its reciprocity estimated and run time.

	100 m	50 m	25 m	Reciprocity estimated	Reciprocity run
Podvin (1991)	1.171 s	2.052 s	10.416 s	3 h 38 min 12 s	3 h 22 min 38 s
Jeong (2008)	0.379 s	1.132 s	8.211 s	2 h 52 min 5 s	2 h 43 min 25 s
Noble (2014)	0.808 s	3.747 s	22.794 s	7 h 57 min 32 s	7 h 12 min 34 s

Second scheme

Results about the second scheme appear on Figure 10 from acquisition geometry shown on Figure 3. It is used three geometry circles with 7, 10 and 13 km of radius shown in Figures 10 a), b) and c) respectively. Each gather reveals the results of travel times difference between analytical equation at the same error scale.

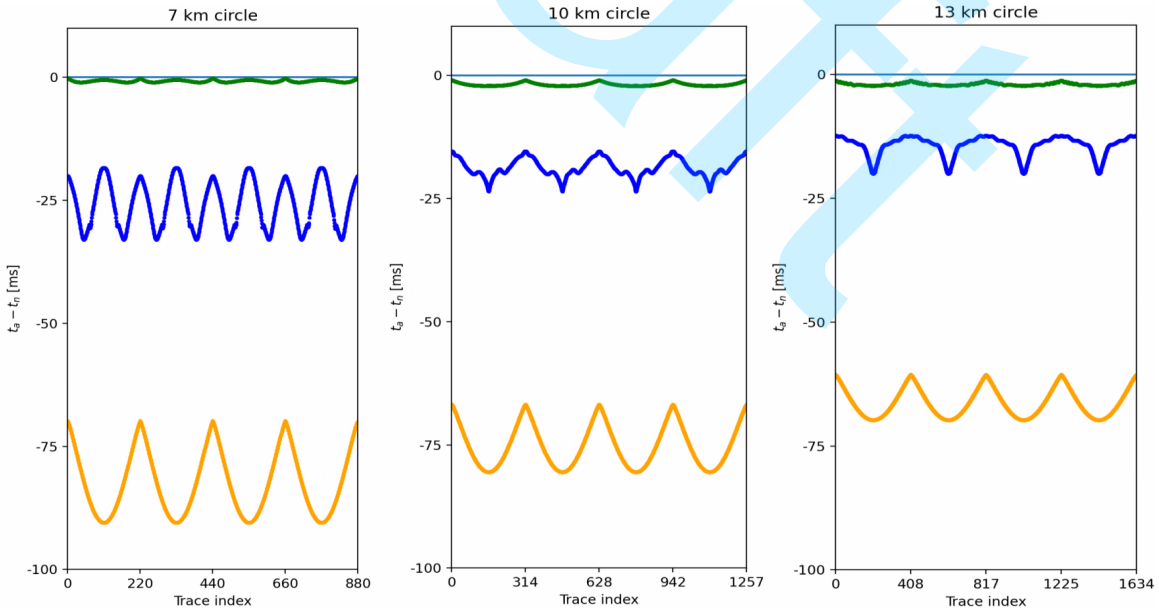

(a) (b) (c)

Figure 10: Resulting gathers for central shot in approach 2: difference to analytical first arrival travel time. All numerical methods is shown using only model sample spacing of 25 m. a) nearest circle offset with 7 km. b) mid circle offset with 10 km. c) longest offset with 13 km. The line colors indicate each method: blue for Podvin and Lecomte (1991), yellow for Jeong and Whitaker (2008) and green for Noble et al. (2014).

Noble et al. (2014) formulation errors is close to zero and the other ones, Podvin and Lecomte (1991) and Jeong and Whitaker (2008) formulations, have average errors of −25 ms and −80 ms respectively. However, on Figure 10 b) and c), when the wavefront propagates through more interfaces, while the Noble et al. (2014) formulation increase its errors, the Podvin and Lecomte (1991) and the Jeong and Whitaker (2008) formulations decrease their errors. The expected behavior is to decrease the precision with increasing the number of layers.

Table 3: Run time execution for a central shot using approach 2, the model with three interfaces.

Podvin (1991)	Jeong (2008)	Noble (2014)	Model storage
93.055 s	62.491 s	129.303 s	807 MB

The errors observed with Noble et al. (2014) have almost the same scale on Figures 10 a), b) and c). For complex models the result might be as accurate as using simple models. The hardware used to compute run time execution on Tables 1,2, 3 and 4 are the CPU Intel Xeon E-2288G (3.7 GHz) and the GPU Nvidia Quadro 4000 (8 GB). Table 3 shows the run time execution for the three numerical methods using a model with $181 \times 1081 \times 1081$ samples. The Jeong and Whitaker (2008) formulation performs better than the other formulations again.

Third scheme

Figure 11 shows the shot 1 in configuration presented in Figure 4. Four windows (Figure 11 a)) are positioned strategically on seismogram to verify the correlations between first arrivals computed by wave propagation and travel times calculated via eikonal solvers. Figures 11 b), c), d) and e) show the windows with their respective signals, red and green, to point out bad and good correlations with numeric seismic waves. Figures 12, 13 and 14 follow the same pattern to verify all directions of propagation in SEG/EAGE Overthrust model. The target first arrivals registered in seismograms are the first black amplitude because of the zero phase wavelet applied.

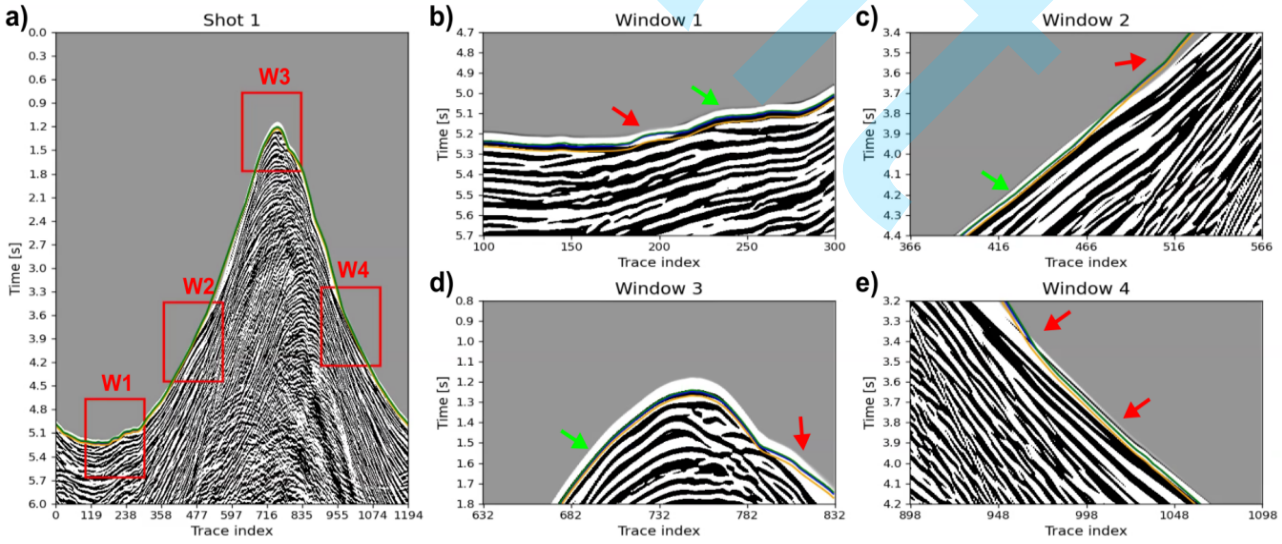

Figure 11: Shot 1 in approach 3. a) 6 seconds of seismic data behavior and all zoom windows are shown at specific p osition. b), c), d) and e) are t he z oom w indows p lot t o s how g ood (green a rrows) and b ad (red a rrows) correlations between seismic data and first arrival travel t imes. T he m ethods are p lotted on b lue (Podvin and Lecomte, 1991), yellow (Jeong and Whitaker, 2008) and green (Noble et al., 2014) lines.

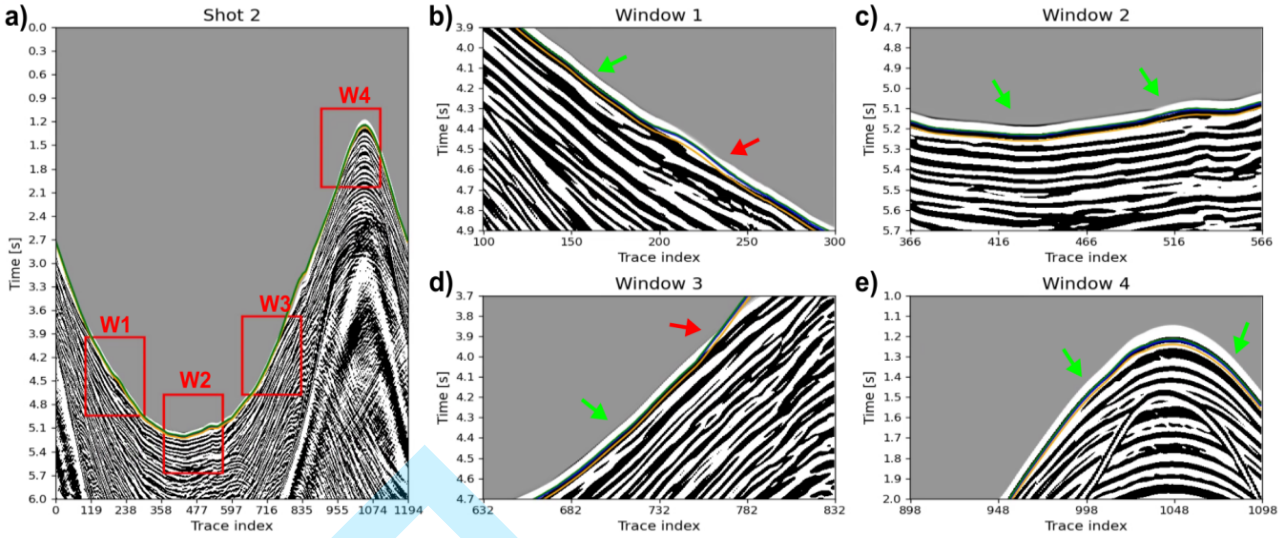

Figure 12: Shot 2 in approach 3. a) 6 seconds of seismic data behavior and all zoom windows are shown at specific position. b), c), d) and e) are the zoom windows plot to show good (green arrows) and bad (red arrows) correlations between seismic data and first arrival travel times. The methods are plotted on blue (Podvin and Lecomte, 1991), yellow (Jeong and Whitaker, 2008) and green (Noble et al., 2014) lines.

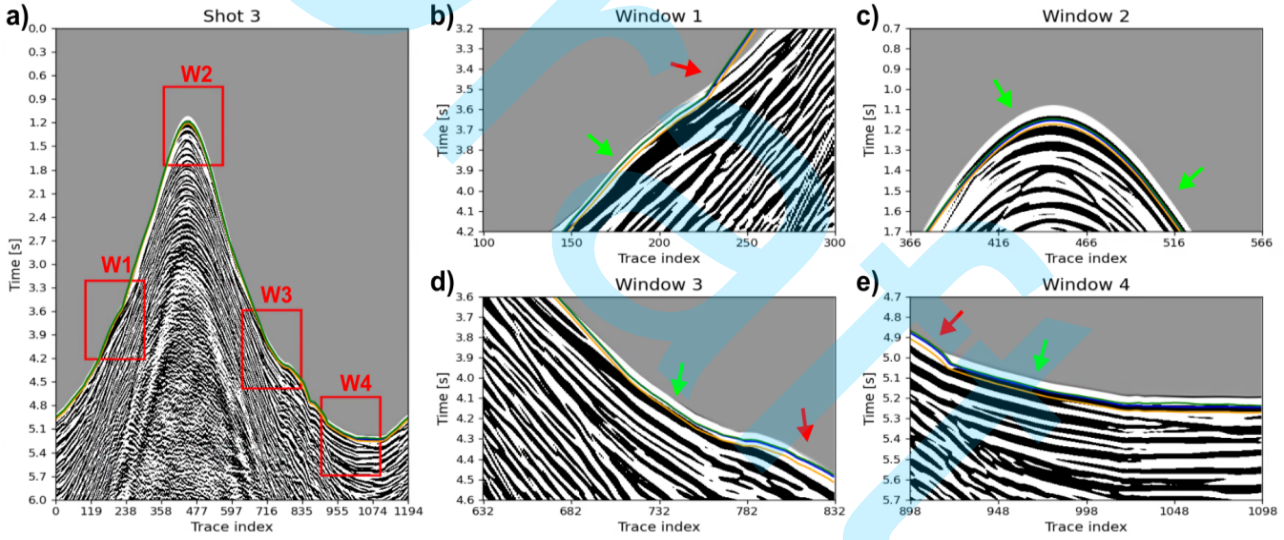

Figure 13: Shot 3 in approach 3. a) 6 seconds of seismic data behavior and all zoom windows are shown at specific position. b), c), d) and e) are the zoom windows plot to show good (green arrows) and bad (red arrows) correlations between seismic data and first arrival travel times. The methods are plotted on blue (Podvin and Lecomte, 1991), yellow (Jeong and Whitaker, 2008) and green (Noble et al., 2014) lines.

A visual correlation is done and we noticed that in nearest offsets a good correlation between seismic and the numerical first arrivals appear in Figures 12 e), 13 c) and 14 b). Only in Figure 11 d), the nearest offsets have anomalous travel times showing smaller results than the finite difference solution for complete wave equation. The bad correlations might be caused by the thin layers in model. The eikonal equation may represent that high velocity thin layers better than the complete finite difference wave equation solution using maximum frequency of 50 Hz. Long offsets have good correlation as show in Figure 12 c), but not in Figures 11 b), 13 e) and 14 d). The most part of correlation, pointed with green arrows, are good, although some red arrows show bad

correlations in near and far offsets. In general considering low frequency wave propagation, high offsets and a model with high velocity thin layers, the correlation between wave equation and eikonal solvers is acceptable for seismic applications.

To verify performance, the comparison between numerical methods run time, inclusive the wave equation solver algorithm and the model size in MB, are shown in Table 4. Computationally, is cheaper solve eikonal equation than acoustic wave equation. Due to the computational effort required to run methods, the hardware used to execute program are now the CPU Intel Xeon Gold 6248R (3.0 GHz) and the GPU Quadro RTX 6000 (22 GB).

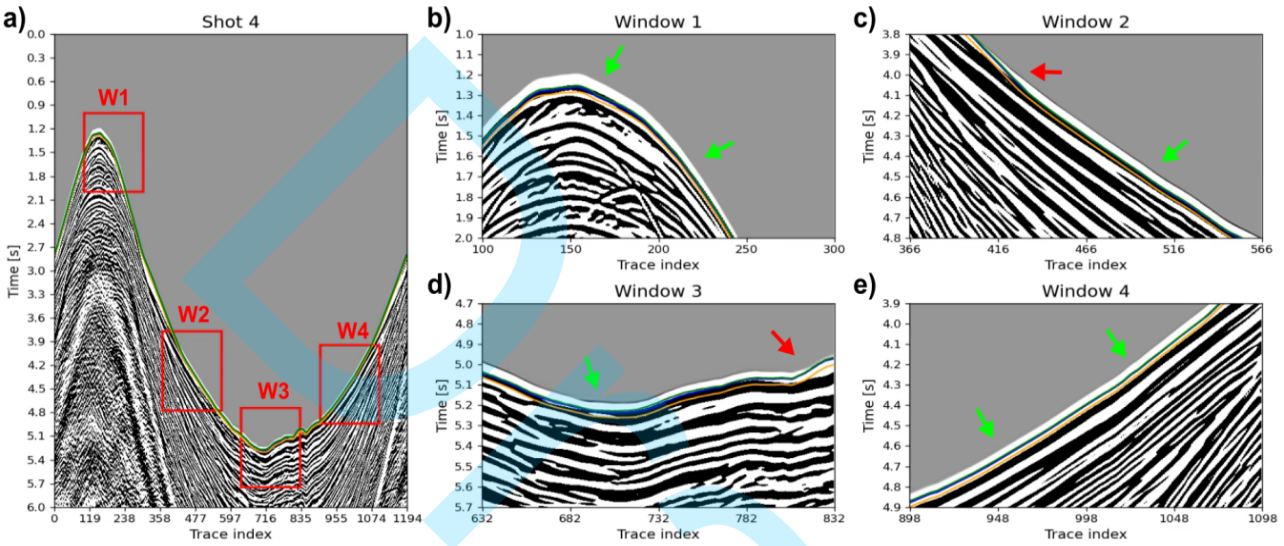

Figure 14: Shot 4 in approach 3. a) 6 seconds of seismic data behavior and all zoom windows are shown at specific position. b), c), d) and e) are the zoom windows plot to show good (green arrows) and bad (red arrows) correlations between seismic data and first arrival travel times. The methods are plotted on blue (Podvin and Lecomte, 1991), yellow (Jeong and Whitaker, 2008) and green (Noble et al., 2014) lines.

Table 4: Four shots run time comparison for approach 3 including wave equation solver and model size.

Podvin (1991)	Jeong (2008)	Noble (2014)	Wave equation	Model storage
39 min 40 s	34 min 50 s	40 min 28 s	3 h 5 min 27 s	3647 MB

The Figure 15 shows the difference between Noble et al. (2014) formulation and the other methods. For each shot, the travel times of the modified Fast Sweeping method is subtracted by the classic and the Fast Iterative method. A mean error per shot is done collecting the travel times per trace and dividing by the total number of traces. The average difference between Noble et al. (2014) and Podvin and Lecomte (1991) formulations is smaller than the difference from Noble et al. (2014) and Jeong and Whitaker (2008) ones. The travel time differences are always negative, so the methods present the same aspects shown in approaches 1 and 2. Podvin and Lecomte (1991) present better results for high contrast model with a mean difference of -6 ms. The Fast Iterative Method travel times present a higher mean error and it can cause wrong seismic analysis when used as a kernel of some methodology.

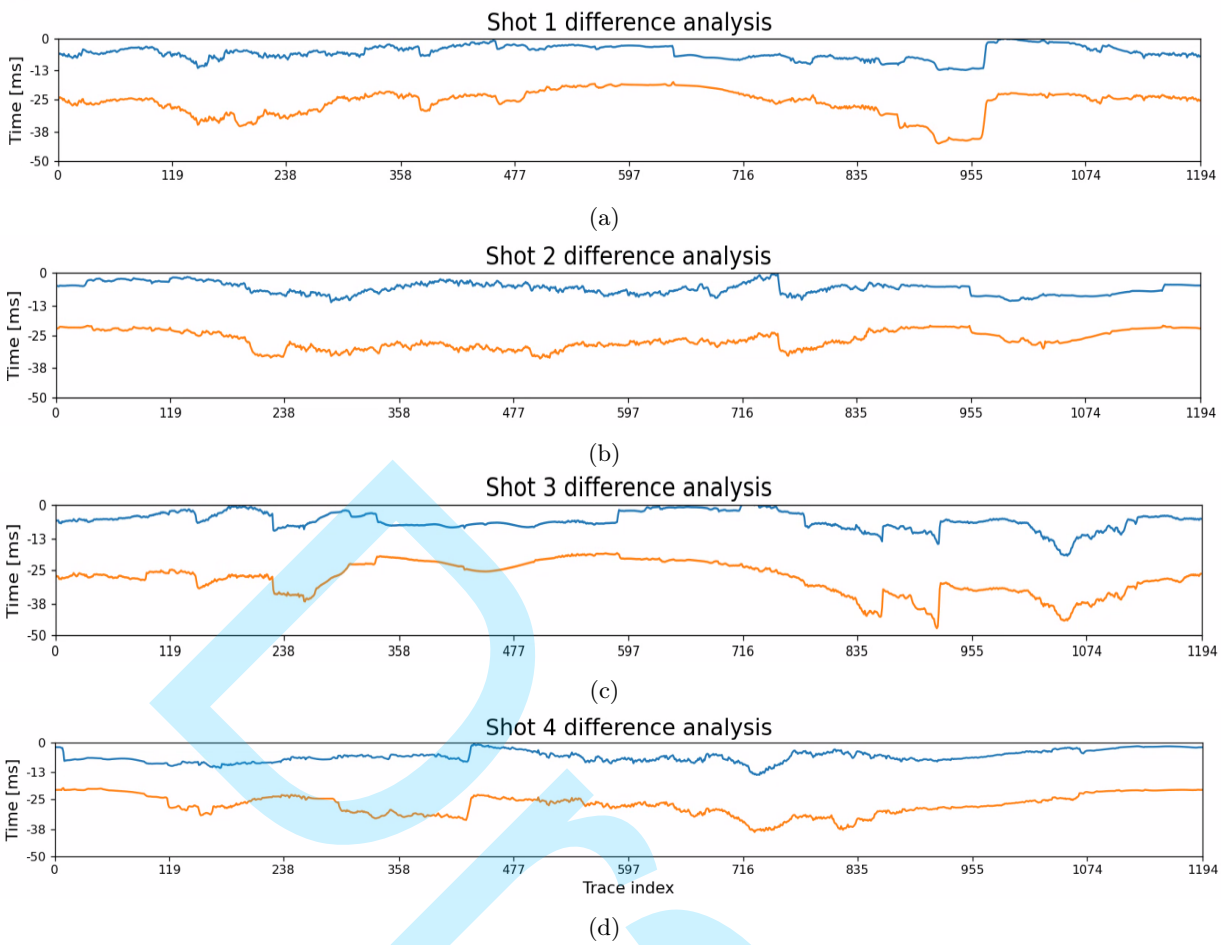

Figure 15: Comparison of differences between Noble et al. (2014) with Podvin and Lecomte (1991) and Jeong and Whitaker (2008) formulations to verify the travel time discrepancy assuming Noble et al. (2014) as the most accurate solver. The difference in milliseconds are negative, in other words, the classic and the Fast Iterative method present a travel time higher than the Fast Sweeping method.

CONCLUSION

From the results among comparisons with Podvin and Lecomte (1991), Jeong and Whitaker (2008), and Noble et al. (2014) formulations for solve eikonal equation, the most accurate method is presented as the modified Fast Sweeping Method. Three approaches are applied and, in large scale situations, as shown in approach 3, the most accurate method does not differ too much in performance from the others. Then this Fast Sweeping Method can be applied on huge simulations. The classic method, shows great differences among reference travel time in approaches 1 and 2. However, for approach 3, with a complex model, Podvin and Lecomte (1991) formulation does not exhibit significant differences from the most accurate solver. Then, the classic formulation still appears as a great eikonal solver in strongly heterogeneous media. The Fast Iterative Method demonstrates the highest performance and a smaller precision in all studied cases. So, this method might be used when the travel times precision is not necessary such as pathfinding problem. A future work suggestion is to verify the improved Fast Iterative Method solution to check accuracy compared with the GPU implementation of the accurate Fast Sweeping Method. Accuracy and performance on seismic imaging experiments such as tomography or depth migration could be taken into account to verify the best method applicability.

ACKNOWLEDGMENTS

The first author from Federal Fluminense University (UFF) gratefully acknowledge the master scholarship provided by the R&D "Refraction seismic for pre-salt reservoirs" (ANP nº 21727-3) project at UFF from Shell Brasil Petróleo Ltda and the strategic importance of the support given by National Agency for Petroleum (ANP) through the R&D levy regulation. The author would like to thank the Seismic Imaging and Seismic Inversion Group (GISIS) team for all knowledge shared and also would like to thank UFF and Oceans and Earth Dynamics graduate program (PPGDOT) for the all infrastructure to develop this work. Also, the author would like to thank Rodrigo S. Stern (UFF/GISIS) for the crucial IT support.

DATA AND MATERIALS AVAILABILITY

The first approach, using a simple model to verify symmetry and accuracy, is the experiment presented in an expanded abstract applied on IX Brazilian Geophysical Symposium. The paper is stored on the official Brazilian Geophysical Society website and the codes used to compute first arrivals are in author's GitHub repository as the experiment presented in the Symposium. The classical method can be found in the global-search earthquake Location in 3D media GitHub repository, the Fast Iterative Method original code can be found in structured eikonal GitHub repository and the accurate fast sweeping method can be found in FTeik-Eikonal-Solver GitHub repository. Recently the Fast Iterative Method original code was integrated in the author's github repository and the Accurate Fast sweeping method was improved in performance, so future works are coming soon.

REFERENCES

Ahmed, S., S. Bak, J. McLaughlin, and D. Renzi, 2011, A third order accurate fast marching method for the eikonal equation in two dimensions: SIAM Journal on Scientific Computing, **33**, 2402–2420, doi: https://doi.org/10.1137/10080258X.

Alkhalifah, T., and S. Fomel, 2001, Implementing the fast marching eikonal solver: spherical versus cartesian coordinates: Geophysical Prospecting, **49**, 165–178, doi: https://doi.org/10.1046/j.1365-2478.2001.00245.x.

Bak, S., J. McLaughlin, and D. Renzi, 2010, Some improvements for the fast sweeping method: SIAM Journal on Scientific Computing, **32**, 2853–2874, doi: https://doi.org/10.1137/090749645.

Balkaya, Ç., Z. Akçığ, and G. Göktürkler, 2010, A comparison of two travel-time tomography schemes for crosshole radar data: Eikonal-equation-based inversion versus ray-based inversion: Journal of Environmental & Engineering Geophysics, **15**, 203–218, doi: https://doi.org/10.2113/JEEG15.4.203.

Bording, R. P., 2004, Finite difference modeling - nearly optimal sponge boundary conditions: Presented at the 2004 SEG Annual Meeting, SEG Technical Program Expanded Abstracts. Denver, Colorado. doi: https://doi.org/10.1190/1.1845189.

Bulhões, F. C., M. A. C. Santos, L. A. Santos, and V. T. X. de Almeida, 2021, Regularization effects on 2D seismic refraction tomography: case study on shallow marine environment: Presented at the 17th International Congress of the Brazilian Geophysical Society, SBGf. Rio de Janeiro, Brazil.

Cai, W., P. Zhu, and G. Li, 2023, Improved fast iterative method for higher calculation accuracy of traveltimes: Computers & Geosciences, **174**, 105331, doi: https://doi.org/10.1016/j.cageo.2023.105331.

Capozzoli, A., C. Curcio, A. Liseno, and S. Savarese, 2013, A comparison of fast marching, fast sweeping and fast iterative methods for the solution of the eikonal equation: 2013 21st Telecommunications Forum Telfor (TELFOR), IEEE, Belgrade, Serbia, 685–688. doi: https://doi.org/10.1109/TELFOR.2013.6716321.

Cerjan, C., D. Kosloff, R. Kosloff, and M. Reshef, 1985, A nonreflecting boundary condition for discrete acoustic and elastic wave equations: Geophysics, **50**, 705–708, doi: https://doi.org/10.1190/1.1441945.

Cervenỳ, V., 2001, Seismic ray theory: Cambridge University Press, Cambridge, doi: https://doi.org/10.1017/CBO9780511529399.

Costa, F., F. Capuzzo, A. de Souza Jr, R. Moreira, J. Lopez, and M. Cetale, 2020, Understanding refracted wave paths for Brazilian pre-salt target-oriented imaging, *in* SEG Technical Program Expanded Abstracts 2020. Virtual event: Society of Exploration Geophysicists, 2375–2380. doi: https://doi.org/10.1190/segam2020-3426868.1.

Da Silva, S., A. Karsou, R. Moreira, J. Lopez, and M. Cetale, 2022, Klein-Gordon equation and variable density effects on acoustic wave propagation in Brazilian pre-salt fields: 83rd EAGE Annual Conference & Exhibition, European Association of Geoscientists & Engineers, Madrid, 1–5. doi: https://doi.org/10.3997/2214-4609.202210385.

Dang, F., and N. Emad, 2014, Fast iterative method in solving eikonal equations: a multi-level parallel approach: Procedia Computer Science, **29**, 1859–1869, doi: https://doi.org/10.1016/j.procs.2014.05.170.

De Matteis, R., A. Romeo, G. Pasquale, G. Iannaccone, and A. Zollo, 2010, 3D tomographic imaging of the southern apennines (Italy): A statistical approach to estimate the model uncertainty and resolution: Studia Geophysica et Geodaetica, **54**, 367–387, doi: https://doi.org/10.1007/s11200-010-0022-x.

Detrixhe, M., F. Gibou, and C. Min, 2013, A parallel fast sweeping method for the eikonal equation: Journal of Computational Physics, **237**, 46–55, doi: https://doi.org/10.1016/j.jcp.2012.11.042.

Farber, R., 2016, Parallel programming with openacc: Newnes, doi: https://doi.org/10.1016/B978-0-12-410397-9.00001-9.

Farra, V., 1993, Ray tracing in complex media: Journal of Applied Geophysics, **30**, 55–73, doi: https://doi.org/10.1016/0926-9851(93)90018-T.

Herrmann, M., 2003, A domain decomposition parallelization of the fast marching method: Technical Report: Presented at the Defense Technical Information Center.

Hicks, G. J., 2002, Arbitrary source and receiver positioning in finite-difference schemes using Kaiser windowed sinc functions: Geophysics, **67**, 156–165, doi: https://doi.org/10.1190/1.1451454.

Hole, J., and B. Zelt, 1995, 3-D finite-difference reflection traveltimes: Geophysical Journal International, **121**, 427–434, doi: https://doi.org/10.1111/j.1365-246X.1995.tb05723.x.

Hong, S., and W.-K. Jeong, 2016, A multi-gpu fast iterative method for eikonal equations using on-the-fly adaptive domain decomposition: Procedia Computer Science, **80**, 190–200, doi: https://doi.org/10.1016/j.procs.2016.05.309.

Huang, G., and S. Luo, 2020, Hybrid fast sweeping methods for anisotropic eikonal equation in two-dimensional tilted transversely isotropic media: Journal of Scientific Computing, **84**, 1–30, doi: https://doi.org/10.1007/s10915-020-01280-3.

Huang, Y., 2021, Improved fast iterative algorithm for eikonal equation for GPU computing (version 3): arXiv,

doi: https://doi.org/10.48550/ARXIV.2106.15869.

Jeong, W.-K., and R. T. Whitaker, 2008, A fast iterative method for eikonal equations: SIAM Journal on Scientific Computing, **30**, 2512–2534, doi: https://doi.org/10.1137/060670298.

Kearey, P., M. Brooks, and I. Hill, 2002, An introduction to geophysical exploration, **4**: John Wiley & Sons.

Koketsu, K., 2000, Finite difference traveltime calculation for head waves travelling along an irregular interface: Geophysical Journal International, **143**, 729–734, doi: https://doi.org/10.1046/j.1365-246X.2000.00269.x.

Lecomte, J., E. Campbell, and J. Letouzey, 1994, Building the *SEG/EAGE* overthrust velocity macro model: EAGE/SEG Summer Workshop-Construction of 3-D Macro Velocity-Depth Models, European Association of Geoscientists & Engineers, cp–96. doi: https://doi.org/10.3997/2214-4609.201407587.

Linde, N., A. Tryggvason, J. E. Peterson, and S. S. Hubbard, 2008, Joint inversion of crosshole radar and seismic traveltimes acquired at the south oyster bacterial transport site: Geophysics, **73**, G29–G37, doi: https://doi.org/10.1190/1.2937467.

Lopez, J., F. Neto, M. Cabrera, S. Cooke, S. Grandi, and D. Roehl, 2020, Refraction seismic for pre-salt reservoir characterization and monitoring: Presented at the SEG International Exposition and Annual Meeting. Virtual event, SEG Technical Program Expanded Abstracts. doi: https://doi.org/10.1190/segam2020-3426667.1.

Luo, S., and J. Qian, 2012, Fast sweeping methods for factored anisotropic eikonal equations: multiplicative and additive factors: Journal of Scientific Computing, **52**, 360–382, doi: https://doi.org/10.1007/s10915-011-9550-y.

Noble, M., A. Gesret, and N. Belayouni, 2014, Accurate 3-D finite difference computation of traveltimes in strongly heterogeneous media: Geophysical Journal International, **199**, 1572–1585, doi: https://doi.org/10.1093/gji/ggu358.

Podvin, P., and I. Lecomte, 1991, Finite difference computation of traveltimes in very contrasted velocity models: a massively parallel approach and its associated tools: Geophysical Journal International, **105**, 271–284, doi: https://doi.org/10.1111/j.1365-246X.1991.tb03461.x.

Qin, F., Y. Luo, K. B. Olsen, W. Cai, and G. T. Schuster, 1992, Finite-difference solution of the eikonal equation along expanding wavefronts: Geophysics, **57**, 478–487, doi: https://doi.org/10.1190/1.1443263.

Rawlinson, N., and M. Sambridge, 2004, Wave front evolution in strongly heterogeneous layered media using the fast marching method: Geophysical Journal International, **156**, 631–647, doi: https://doi.org/10.1111/j.1365-246X.2004.02153.x.

Rawlinson, N., and M. Sambridge, 2005, The fast marching method: an effective tool for tomographic imaging and tracking multiple phases in complex layered media: Exploration Geophysics, **36**, 341–350, doi: https://doi.org/10.1071/EG05341.

Robinson, E. A., and D. Clark, 2017, Basic geophysics: Society of Exploration Geophysicists. Geophysical Monograph Series, 22, 376 pp, doi: https://doi.org/10.1190/1.9781560803461.

Sethian, J. A., 1999, Fast marching methods: SIAM review, **41**, 199–235, doi: https://doi.org/10.1137/S0036144598347059.

Shen, Y., and J. Zhang, 2020, Refraction wavefield migration: Geophysics, **85**, Q27–Q37, doi: https://doi.org/10.1190/geo2020-0141.1.

Sheriff, R. E., and L. P. Geldart, 1995, Exploration seismology: Cambridge University Press, doi: https://doi.org/10.1017/CBO9781139168359.

Tryggvason, A., and B. Bergman, 2006, A traveltime reciprocity discrepancy in the Podvin & Lecomte *time3d* finite difference algorithm: Geophysical Journal International, **165**, 432–435, doi: https://doi.org/10.1111/j.1365-246X.2006.02925.x.

Van Trier, J., and W. W. Symes, 1991, Upwind finite-difference calculation of traveltimes: Geophysics, **56**, 812–821, doi: https://doi.org/10.1190/1.1443099.

Vidale, J., 1988, Finite-difference calculation of travel times: Bulletin of the Seismological Society of America, **78**, 2062–2076, doi: 10.1785/BSSA0780062062.

Waheed, U. B., and T. Alkhalifah, 2017, A fast sweeping algorithm for accurate solution of the tilted transversely isotropic eikonal equation using factorization: Geophysics, **82**, WB1–WB8, doi: https://doi.org/10.1190/geo2016-0712.1.

Waheed, U. B., C. E. Yarman, and G. Flagg, 2015, An iterative, fast-sweeping-based eikonal solver for 3D tilted anisotropic media: Geophysics, **80**, C49–C58, doi: https://doi.org/10.1190/geo2014-0375.1.

White, M. C., H. Fang, N. Nakata, and Y. Ben-Zion, 2020, Pykonal: a python package for solving the eikonal equation in spherical and Cartesian coordinates using the fast marching method: Seismological Research Letters, **91**, 2378–2389, doi: https://doi.org/10.1785/0220190318.

Yang, J., and F. Stern, 2017, A highly scalable massively parallel fast marching method for the eikonal equation: Journal of Computational Physics, **332**, 333–362, doi: https://doi.org/10.1016/j.jcp.2016.12.012.

Yordkayhun, S., A. Tryggvason, B. Norden, C. Juhlin, and B. Bergman, 2009, 3D seismic traveltime tomography imaging of the shallow subsurface at the CO2SINK project site, Ketzin, Germany: Geophysics, **74**, G1–G15, doi: https://doi.org/10.1190/1.3026553.

Zhao, H., 2005, A fast sweeping method for eikonal equations: Mathematics of Computation, **74**, 603–627, doi: https://doi.org/10.1090/S0025-5718-04-01678-3.

Zhao, H., 2007, Parallel implementations of the fast sweeping method: Institute of Computational Mathematics and Scientific / Engineering Computing, 25, 4, 421–429, doi: https://www.jstor.org/stable/43693378.

Alves, P. H. B.: code development, methodology, writing - original draft, review & editing; **Santos, L. A.**: writing - review & editing; **Capuzzo, F. V.:** initial code development; **Cetale, M.**: writing - review & editing.